

AC: some of the pages are cluttered with comments, so we could not add an answer beneath or near each of them. Instead, we provided the answers in the same order as they appear in the top of the page. Sometimes, as on this page, one answer covers several questions.

<https://doi.org/10.5194/amt-2021-96>
Preprint. Discussion started: 19 April 2021
© Author(s) 2021. CC BY 4.0 License.



Comparing scattering ratio products retrieved from ALADIN/Aeolus and CALIOP/CALIPSO observations: sensitivity, comparability, and temporal evolution

Artem G. Feofilov¹, Hélène Chepfer¹, Vincent Noel², Rodrigo Guzman¹, Cyprien Gindre¹ and Marjolaine Chiriaco³

¹LMD/IPSL, Sorbonne Université, UPMC Univ. Paris 06, CNRS, École polytechnique, Palaiseau, 91128, France

²Laboratoire d'Aérodynamique, CNRS/UPS, Observatoire Midi-Pyrénées, 14 avenue Edouard Belin, Toulouse, France

³LATMOS/IPSL, Univ. Versailles Saint-Quentin en Yvelines, Guyancourt, France

Correspondence to: Artem G. Feofilov (artem.feofilov@lmd.polytechnique.fr)

Abstract.

The spaceborne active sounders have been contributing invaluable vertically resolved information of atmospheric optical properties since the launch of CALIPSO (Cloud-Aerosol Lidar and Infrared Pathfinder Satellite Observation) in 2006. To ensure the continuity of climate studies and monitoring the global changes, one has to understand the differences between lidars operating at different wavelengths, flying at different orbits, and utilizing different observation geometries, receiving paths, and detectors. In this article, we show the results of an intercomparison study of ALADIN (Atmospheric Laser Doppler Instrument) and CALIOP (Cloud-Aerosol Lidar with Orthogonal Polarization) lidars using their scattering ratio (SR) products for the period of 28/06/2019–31/12/2019. We suggest an optimal set of collocation criteria ($\Delta\text{dist} < 1^\circ$, $\Delta\text{time} < 6\text{h}$), which would give a representative set of collocated profiles and we show that for such a pair of instruments the theoretically achievable cloud detection agreement for the data collected with aforementioned criteria is 0.77 ± 0.17 . The analysis of a collocated database consisting of ~78000 pairs of collocated nighttime SR profiles revealed the following: (a) in the cloud-free area, the agreement is good indicating low frequency of false positive cloud detections by both instruments; (b) the cloud detection agreement is better for the lower layers. Above ~7 km, the ALADIN product demonstrates lower sensitivity because of lower backscatter at 355 nm and because of lower signal-to-noise ratio; (c) in 50% of the analyzed cases when ALADIN reported a low cloud not detected by CALIOP, the middle level cloud hindered the observations and perturbed the ALADIN's retrieval indicating the need for quality flag refining for such scenarios; (d) large sensitivity to lower clouds leads to skewing the ALADIN's cloud peaks down by ~0.5 ± 0.4 km, but this effect does not alter the polar stratospheric cloud peak heights; (e) temporal evolution of cloud agreement quality does not reveal any anomaly for the considered period, indicating that hot pixels and laser degradation effects in ALADIN have been mitigated at least down to the uncertainties in the following cloud detection agreement values: $61 \pm 16\%$, $34 \pm 18\%$, $24 \pm 10\%$, $26 \pm 12\%$ at 0.75 km, 2.25 km, 6.75 km, 8.75 km, and 10.25 km respectively.

Comments on amt-

Page: 1

Author: Subject: Sticky Note Date: 14/06/2021 09:43:49

Abstract not understandable

Author: Subject: Comment on Text Date: 14/06/2021 09:44:08

poor phrasing

Author: Subject: Comment on Text Date: 14/06/2021 11:26:31

What do these numbers mean? It is not understandable without reading the paper

AC: we have rewritten the abstract and we introduced the normalized cloud detection agreement, CDAnorm, in the Abstract



1 Introduction

Clouds play an important role in the energy budget of our planet: optically thick clouds reflect the incoming solar radiation, leading to cooling of the Earth, while thinner clouds act as “greenhouse films”, preventing escape of the Earth’s long-wave radiation to space. Climate feedback analyses reveal that clouds are a large source of uncertainty for the climate sensitivity of climate models and, therefore, for the predicted climate development scenarios (e.g. Nam et al., 2012; Chepfer et al., 2014; Vaillant de Guélis et al., 2018). Understanding the Earth’s radiative energy budget requires knowing the cloud cover, their geographical and altitudinal distribution, temperature, composition, as well as the optical properties of cloud particles and their concentration.

Satellite observations have been providing a continuous survey of clouds over the whole globe. IR sounders have been observing our planet since 1979: from the TOVS (TIROS Operational Vertical Sounder) instruments (Smith et al., 1979) onboard the NOAA polar satellites to the AIRS (Atmospheric InfraRed Sounder) spectrometer (Chahine et al., 2006) onboard Aqua (since 2002) and to the IASI (Infrared Atmospheric Sounding Interferometer) instrument (Chalon et al., 2001; Hilton et al., 2012) onboard MetOp (since 2006), with increasing spectral resolution. Despite an excellent daily coverage and daytime/nighttime observation capability (Menzel et al., 2016; Stuberneau et al., 2017), the height uncertainty of the cloud products retrieved from the observations performed by these spaceborne instruments is limited by the width of their channels’ contribution functions, which is on the order of hundreds of meters, and the vertical profile of the cloud cannot be retrieved with accuracy needed for climate feedback analysis. This drawback is eliminated by active sounders, the very nature of which is based on altitude-resolved detection of backscattered radiation, and the vertical profiles of the cloud parameters are available from the CALIOP (Cloud-Aerosol Lidar with Orthogonal Polarization) lidar (Winker et al., 2003) and CloudSat radar (Stephens et al., 2002) since 2006, CATS (Cloud-Aerosol Transport System) lidar on-board ISS provided measurements for over 33 months starting from the beginning of 2015 (McGill et al., 2015). The ALADIN (Atmospheric Laser Doppler Instrument) lidar on-board Aeolus (Krawczyk et al., 1995; Stoffelen et al., 2005; ADM-Aeolus Science report, 2008) has been measuring horizontal winds and aerosol/clouds since September 2018. More lidars are planned – in 2023, the ATLAS (Atmospheric Lidar)/EarthCare instrument (Hélière et al., 2012) will be launched and other space-borne lidars are in the development phase. Even though all active instruments share the same measuring principle – a short pulse of laser or radar electromagnetic radiation is sent to the atmosphere and the time-resolved backscatter signal is collected by the telescope and is registered in one or several receiver channels, the wavelength, pulse energy, pulse repetition frequency (PRF), telescope diameter, orbit, detector, and many other parameters are not the same for any given pair of current or future instruments. These differences are responsible for the active instruments’ capability of detecting atmospheric aerosols and/or hydrometeors for given atmospheric scenario and observation conditions (day, night, averaging distance). At the same time, there is an obvious need of ensuring the continuity of global spaceborne measurements and obtaining a seamless transition between the satellite missions (Chepfer et al., 2018).

Author:	Subject: Comment on Text	Date: 14 06 2021 09:45:08
Author:	Subject: Sticky Note	Date: 17 05 2021 14:56:29
Author:	Subject: Highlight	Date: 17 05 2021 14:59:05

This work seeks to address this issue using ALADIN/Aeolus spaceborne wind lidar operating at 355 nm and CALIOP/CALIPSO atmospheric lidar operating at 532 nm. Even though the main goal of ALADIN is wind detection (Reitebuch et al., 2020; Straume et al., 2020), the calibration of which does not rely on absolute calibration of the detected radiation, its products include atmospheric optical properties and such a comparison serves the inter-calibration purposes. In addition, the methods developed in the course of this study, and the interpretation of the results will set the stage for the future validation of the ATLID/EarthCare instrument and other spaceborne lidars.

The structure of the article is as follows. In Section 2, we describe the datasets used in this study, explain the collocation criteria, and provide an estimate of the best possible theoretically achievable agreement for two instruments in given configuration. In Section 3, we strive to provide a multifaceted view of the collocated dataset and discuss the observed differences. Section 4 concludes the article.

2 Datasets and methods

We start this section with the description of ALADIN/Aeolus optical properties dataset followed by the description of CALIOP/CALIPSO product and its modification aimed at matching the sampling and averaging of Aeolus product. In the next steps, we define the procedures and criteria for the comparison of these two products.

2.1 AEOLUS

A detailed description of the Aeolus mission and its instrument can be found in (Krawczyk et al., 1995; Hoffelen et al., 2005; ADM-Aeolus Science report, 2008; Flamant et al., 2017) and here we provide only a brief description of the lidar and the details necessary for understanding the key differences between the compared instruments. The Aeolus satellite carries a Doppler wind lidar called ALADIN, which operates at 355 nm wavelength and is composed of a transmitter, a Cassegrain telescope, and a receiver capable of separating the molecular (Rayleigh) and particulate (Mie) backscattered photons (HSRL, high spectral resolution lidar). The lidar is aimed 35° from nadir and 90° to the satellite track. Its orbit is inclined at 96.97° and the instrument overpasses the equator at 6h and 18h of local solar time (LST), see also Table 1 to compare with CALIOP. The laser emitter sends 15 ns long pulses of 355 nm radiation down into the atmosphere 30 times per second. The telescope collects the light that is backscattered from air molecules, aerosols and hydrometeors. The received backscatter signal in Mie receiver passes through a Fizeau interferometer, which produces a linear fringe whose position on the ACCD (Accumulation Charge Coupled Device) detector of this channel is linked to the wind velocity. As for the Rayleigh receiver, it uses a dual-filter Fabry-Pérot interferometer, which throws two images on the ACCD detector of this channel, and the wind speed is defined from the ratio of intensity of these two images (Chazin et al., 1989). Besides the winds, the Aeolus processing algorithms retrieve the optical properties of the observed atmospheric layers (Ansmann et al., 2007; Flamant et al., 2017). The vertical resolution of the instrument is adjustable, but the total number of points in a vertical profile is defined by a number of rows of the detector dedicated to this purpose (24). The observation priorities changed throughout the period of the mission

AC: we have rewritten and reorganized the text and we added a whole new section with definitions (Section 3). As for the phrase with "set the stage", we have rewritten it to "In addition, the methods developed in this study and its conclusions will set the stage for the future comparison of the ATLID/EarthCare observations with other space-borne lidar". We cannot be more specific at this time.

AC: In the updated version of the manuscript, Section 3 is dedicated to the definitions and the SR conversion approach

AC: we did not get, why the PRF of 50Hz is marked.

95 (Bley et al., 2021), and for the majority of the period considered in this work (see below), the vertical sampling of both Mie and Rayleigh channels between 2 km and 22 km was equal to 1 km whereas the sampling below 2 km varied from 0.25 to 1 km. The native horizontal resolution of 140 m of the instrument is sacrificed to achieve a higher signal to noise ratio both onboard by accumulating the detected profiles and on the ground by averaging the downloaded profiles at different steps of the processing chain (Flamant et al., 2017).

100 The present study has been done using the pilot L2A dataset from Aeolus, **Prototype v3.10, which is available for a limited period of ALADIN's observations, from 28/06/2019 through the 31/12/2019**. According to (Flamant et al., 2017), the L2A data is produced from the L1B product of this instrument and it contains height profiles of Mie and Rayleigh co-polarized backscatter and extinction coefficients, **scattering ratios**, and lidar ratios (Flamant et al., 2008; Lolli et al., 2013) along the lidar line-of-sight. For the end user, the profiles are provided both on observation scale (87 km averages) and on smaller scales after applying scene classification, but for the purposes of the present work the scattering ratio on the scale of 87 km is an original choice.

105 In Fig. 1(a-c), we show the observation geometry and sampling of ALADIN's L2A product as well as three variables retrieved from its observations, namely: the APB (Attenuated Particular Backscatter), the AMB (Attenuated Molecular Backscatter), and the ATB (Attenuated Total Backscatter). The white dashed lines in Fig. 1 represent the line of sight of the instrument. One has to note, however, that in the real life the ALADIN's line of sight is pointed perpendicular to the flight direction; at the same time, **the horizontal variability of the observed scene is nearly the same in latitudinal and longitudinal directions** at 100 km distance, so the sketch gives an idea of the comparability of the physical parameters observed by ALADIN (Fig. 1a-c) and CALIOP (Fig. 1d). The atmospheric scene used in Fig. 1 has been calculated for demonstration purposes for two wavelengths, 355 nm (Fig. 1a,b,c) and 532 nm (Fig. 1d) from the output of the E-AMV1 (Energy Exascale Earth System Model (E3SM) atmosphere model version 1) atmospheric model (Kasch et al., 2019) **for the conditions of autumn equinox in Northern hemisphere**. This data has been obtained with the help of the COSP2 (the Cloud Feedback Model Intercomparison Project Observational Simulator Package, v2) package, which is capable of simulating the atmospheric observables for spaceborne instruments (Swailes et al., 2018). The CALIOP is built into COSP2 (Chepfer et al., 2008) whereas the ALADIN is not yet a part of this package, so we used our 355 nm calculations by COSP2 (Reverdy et al., 2015) at fine grid corresponding to ALADIN's original laser pulse frequency rate and modified them in accordance with the ALADIN's vertical and horizontal **averaging**. The cloud variability along the satellite's track has been estimated from the gridded EAMV1 data using the **parameterization of Boutle et al. (2014)**. **Figure 1 also serves as an illustration to theoretically achievable cloud detection agreement discussed below**.

120 For each profile corresponding to an inclined dashed line in Fig. 1, we extracted the corresponding scattering ratio (SR) column of **raw optical properties** group of variables where SCA stands for standard correct algorithm (Flamant et al., 2017). An important companion of such a column is a corresponding quality flag column, which we scanned looking for the points characterized either **by high Mie signal-to-noise ratio (SNR) or by high Rayleigh SNR**, and by a flag that indicates an absence

Author:	Subject: Highlight	Date:	14.06.2021 11:05:32
No reference given	You need to explain what this means and what is the difference to operational data		
Author:	Subject: Comment on Text	Date:	18.05.2021 09:52:16
the scattering ratio you use is never defined, as it is essential for this work, you should do so			
Author:	Subject: Comment on Text	Date:	17.05.2021 15:05:39
this is not true and heavily depends on the scene			
Author:	Subject: Comment on Text	Date:	17.05.2021 15:07:53
it gives a wrong idea, because scenes are usually by far not so homogenous			
Author:	Subject: Comment on Text	Date:	17.05.2021 15:08:41
for what do you need the autumn equinox in this simulation?			
Author:	Subject: Comment on Text	Date:	17.05.2021 15:09:42
what does this mean?			
Author:	Subject: Comment on Text	Date:	14.06.2021 09:41:29
I don't understand, more explanation needed	I do not see any cloud in this figure		
Author:	Subject: Comment on Text	Date:	14.06.2021 11:07:13
nobody who is not familiar with Aeolus L2A data structure will understand this			
Furthermore, it is not trace-able/understandable for anyone not within an Aeolus Cal/Val team yet. A proper reference should be given or, if not available, a more detailed description of the data set needs to be given here. E.g., what is the difference to other Aeolus data. Why have you used this data set, etc.			
Author:	Subject: Comment on Text	Date:	14.06.2021 11:06:50
what does this mean: HIGH SNR? >2, >10, >100?			

AC: In the new version, we write "the L2A data is produced from the L1B product of this instrument and it contains height profiles of Mie and Rayleigh co-polarized backscatter and extinction coefficients, scattering ratios (SR), and lidar ratios (Flamant et al., 2017; Lolli et al., 2013) along the lidar line-of-sight". There's no reference per se, this is a test product and we have a corresponding statement in the Disclaimer at the end of the manuscript

AC: Please, see new Section 3

AC: we have updated the description of our numerical experiment

AC: Fig. 1 is now different

AC: There's nothing special about the Autumn equinox itself, this season just happens to be in the middle of the Prototype v3.10 data period.

AC: We got rid of internal Aeolus variable names in the present version of the manuscript

AC: the exact values of SNR used in the Aeolus algorithms are not given in the ATBD, so we just used the binary (yes/no) flags relying on the experience of the processing team.

of signal attenuation. Presumably, **these flags are necessary and sufficient for a valid SR profile**, which can be then compared with that of CALIOP

2.2 CALIPSO-GOCCP

CALIOP, a two-wavelength polarization-sensitive **nadir** viewing lidar, provides high-resolution vertical profiles of **gas** and clouds **its 705 km orbit** is inclined at 98.05° and it overpasses the equator at 1h30 and 13h30 LST, see also Table 1. It uses three receiver channels: one measuring the 1064 nm backscatter intensity and two channels measuring orthogonally polarized components of the 532 nm backscattered signal. Cloud and aerosol layers are detected by comparing the measured 532 nm signal return with the return expected from a molecular atmosphere.

The CALIPSO-GOCCP (GCM Oriented Cloud Calipso Product) was initially designed to evaluate **GCM cloudiness** (Chepfer et al., 2010). It is derived from CALIPSO L1/NASA Products (LMD/IPSL with the support of NASA/CNRS, ICARE, and ClimServ and it contains observational cloud diagnostics including the instantaneous scattering ratio (profiles) at the native horizontal resolution of CALIOP (333 m) and at ~0.5 km vertical resolution. This makes it a good reference dataset for ALADIN retrievals because it can be easily recalculated to the latter's horizontal and vertical grids considering the corresponding horizontal averaging. Since the CALIOP is not a HSRL, the detailed information on AMB and APB is not available, and one has to compare the SR products. Correspondingly, we convert the ALADIN's SR retrieval at 355 nm to SR at 532 nm using the following equation:

$$SR_{532} = SR_{355} \times 3.3 - 2.3 \quad (1)$$

which is derived from (Collis and Russell, 1976) in an assumption that their fitting parameter Λ (see their Section 4.3.1) is equal to 3. The choice of the fitting parameter is not crucial for the purposes of the present work because the conversion described by Eq. 1 is linear and it does not change the altitude distribution of the SR. **On the other hand, using the same physical parameter is highly advisable for the comparisons we are intending to perform. Theoretically, one could have validated the parameters of Eq. 1 using the collocated data under consideration, but, looking ahead, one can say that the spread of the values is too large to do it with reasonable uncertainty, so we will stay with Eq. 1 in the framework of this paper and in Appendix A we justify our choice of conversion coefficients using the collocated data.**

2.3 Collocation criteria

As for any collocation, there is a trade-off between the quality of collocation and the number of collocated pairs of profiles. As we show below, in the case of AEOLUS and CALIPSO, this tradeoff is supplemented with a requirement of a representative geographical coverage, because imposing a strict temporal overlap criterion dramatically changes the latitudinal distribution of the collocated points. Since the horizontal averaging and resolution of the Aeolus Prototype v3.10 product is 87 km, there is no much sense in collocating the data with the accuracy better than this value. On the other hand, a fractional standard deviation f_c of cloud water content at 1° (~111 km) distance is about 0.5 for a cloud cover of 1 (Boutle et al., 2014), and there

Author: Subject: Comment on Text Date: 14.06.2021 11:07:30
 I am not sure if these flags are valid in these kind of data. These data are all preliminary. You should discuss this.

Author: Subject: Comment on Text Date: 18.05.2021 09:56:56
 This statement is in contradiction to Figure 1, where you clearly see that it is not nadir but only close to nadir.

Author: Subject: Comment on Text Date: 18.05.2021 09:56:24
 I guess you mean the altitude of the orbit, but this is not written here. Please state correctly.

Author: Subject: Comment on Text Date: 18.05.2021 10:26:48
 GCM never explained.

Author: Subject: Comment on Text Date: 14.06.2021 09:54:36
 This is not state of the art and not acceptable - see plots in my text.

Author: Subject: Comment on Text Date: 14.06.2021 09:55:42
 I do not understand this statement. And the justification given in the Appendix is not sufficient in my opinion.

AC: the Prototype version of the Aeolus data is supposed to be self-consistent. We have a Disclaimer at the end of the manuscript, which states that all the data in this version are preliminary.

AC: The small offset from nadir in CALIOP was introduced to reduce the surface reflection effects. This modification barely changed the optical path lengths, so it still can be called a "nadir-viewing instrument". To be precise, we changed it to "near nadir viewing lidar".

AC: We modified the phrasing about the orbital height, thanks for pointing this out.

AC: GCM is now introduced in the explanation of the first abbreviation.

AC: We agree that SR recalculation was oversimplified. In the present version of the manuscript, we have a whole new section dedicated to the definitions and recalculation approach.

AC: The validation part and its discussion have been removed.

Author:	Subject: Comment on Text	Date: 14.06.2021 11:07:47
As Aeolus is flying at a dusk-dawn orbit, how can you select night time cases? Or is this valid for Calipso only? But then you have a bias, right?		
Author:	Subject: Comment on Text	Date: 14.06.2021 09:56:04
I really did not understand what you are doing here. Maybe a sketch or flowchart could help		
Why do you need to imitate diurnal variation? Please explain!		
Author:	Subject: Comment on Text	Date: 14.06.2021 11:09:06
The choice of this threshold is not clear to me and seems very arbitrary. Furthermore, the use of a scattering ratio for cloud detection in questionable to me at all, as the scattering ratio depends on temperature and pressure and thus on height even with uniformly distributed particle load as shown in the attached plots. Using one threshold would mean that you detect a cloud at one height while you may not detect a similar cloud at another height. Thus, using the scattering ratio for cloud detection is not appropriate in my opinion. You could have used the scattering ratio from the satellite data to calculate the real particle backscatter coeff by using the molecular backscatter which you calculate from the meteorological data which is included in the satellite data as well		
Author:	Subject: Comment on Text	Date: 18.05.2021 15:10:14
I do not "see" that At least in Fig 3 it is not obvious. To what you are referring to? And can you give more explanation?		
Author:	Subject: Comment on Text	Date: 14.06.2021 10:00:39
Any evidence or proof for such a statement? Again to what are you referring?		
Author:	Subject: Comment on Text	Date: 18.05.2021 15:12:08
is this valid for ALADIN as well?		

is a risk of comparing incoherent quantities, so we took $\Delta \text{dist} = 1^\circ$ as a limit for the collocations and created several subsets based on the Δtime , the absolute value of the difference between two collocated measurements. In Fig. 2, we show three such subsets, and the Table 2 provides the information about the other cases we considered. On the one hand, one can see that a strict collocation criterion of $\Delta \text{time} < 1\text{h}$ (Fig. 2a) provides the information only about two narrow zones in the Southern and Northern polar regions. On the other hand, an excellent geographical coverage shown in Fig. 2c comes at the cost of mixing up the cases, which differ by almost one day that is unacceptable from the point of view of temporal variation. In addition, this case is characterized by unequal distribution of Δtime throughout the globe. Finally, a subset corresponding to $\Delta \text{time} < 6\text{h}$ (Fig. 2b) has been chosen for the analysis. Over the oceans, the diurnal effects in cloud distribution associated with this difference are small (e.g. Noel et al., 2018; Chepfer et al., 2019; Feofilov and Stubenrauch, 2019) and the layer represents one third of the analyzed cases. To avoid the risks associated with the solar contamination, we picked up only the night-time cases which yield about 7 8E4 pairs of SR profiles. In supplementary materials, we provide the complete collocated database, which corresponds to the last line, 4th column of Table 2 (3 7E5 collocations), for further analysis by the interested teams.

2.4 Estimating the theoretically achievable agreement between two collocated datasets

To justify the collocation criteria and to estimate the theoretically possible agreement for the clouds detected by two instruments in a given setup and for the selected Δtime and Δdist values, we have performed a numerical experiment using the same calculated data as we used in Fig. 1. This time, we picked up the "night curtain" at 232 m/s calculated at the resolution of CALIOP (333m) and created artificial pairs of "collocated" data with the Adist distribution modulated by that of a real collocated dataset. The "reference" CALIOP profile has been composed using 2000 individual SR profiles covering 67 km region that is somewhat less than the 87 km covered by ALADIN. This averaging is supposed to match the mean atmospheric properties and at the same time it is not supposed to go so far from the ALADIN footprint to avoid the "test" SR profile was created from the SR averages, considering both by ALADIN's off-nadir pointing and its 87 km averaging. To imitate the diurnal variation, we modulated the SRs using the 6-hour diurnal cycle amplitudes for land and ocean retrieved from active and passive observations (Noel et al., 2019; Chepfer et al., 2019; Feofilov and Stubenrauch, 2019) and added them to the comparison. Besides testing a noise-free simulation, we also checked the effects introduced by instrumental noise for CALIOP. Since ALADIN is not yet part of ECOSP2, we used the estimates from (Vismann et al., 2007). Overall, we considered about 1E5 pairs of pseudo-collocated data and we present the results of cloud detection in Fig. 3. We define the cloud detection agreement as follows: for each altitude bin, the cloud detection agreement is a ratio of a number of cases when both instruments have detected a cloud (SR>3) to a total number of joint observations. For a given altitude bin, the cloud amount is a ratio of number of cases with SR>5 to a total number of profiles for a single instrument, and the normalized cloud detection agreement is a ratio of the former to the latter. As one can see, the normalized cloud detection quality is mostly defined by a horizontal variability of aerosols/hydrometeors and by differences in viewing geometries of two instruments. Observation noise and diurnal variation play the secondary role and according to our estimates the saturation effects in 355 nm and 532 nm channels associated with opaque clouds (Guzman et al., 2017) do not add more than 2% to the cloud detection mismatch (not shown in

AC: Indeed, dusk-dawn observations are not equal to night-time observations, but this selection itself does not lead to a bias. We discuss the diurnal cycle effects in the manuscript and according to our estimates performed without local time filtering, the results are nearly the same. The idea here was to get rid of solar photons and to apply the same SR threshold for both instruments.

AC: A flowchart has been added and the text was updated

AC: As for the choice of the SR threshold, please, see the comments in the text version of the review.

AC: If one looks at Fig. 3 (now Fig. 4), one will see that the curves marked "w/o noise" and "w/noise" are virtually the same. The curves with noise correspond to variability caused by diurnal variation and instrumental noise added to the calculations. Therefore, the primary source of deviation from 1 is the observation geometry and the collocation quality.

AC: Saturation effects do not depend on the instrument

Fig 3 for the sake of clarity) Overall, the theoretically achievable agreement for the collocated data at a given setup can be estimated as 0.77 ± 0.17 for cloud detection

3 Results and discussion

3.1 Zonal averages

To give a general overview of the agreement between **two products**, we have split the database to latitudinal zones: 90S–60S, 60S–30S, 30S–30N, 30N–60N, 60N–90N (Fig. 4). As it was stated above, we rescale the SR_{ALADIN} values retrieved from ALADIN observations to SR_{SR} using Eq. 1. Even though the zonal mean statistics does not imply using collocated data, we do it to avoid any incoherence in sampling different geographic areas. By using exactly the same number of profiles collocated within 1° , we ensure the same coverage and sampling by both lidars. If the detection efficiency of different cloud types were the same for two instruments, the plots would have been close to each other because the horizontal variability of clouds would cancel out due to averaging over a large number of profiles within **the zone** and the diurnal variation is small over oceans, which constitute two thirds of the cases used to **build Fig. 4** (Nesèl et al., 2016; Chepfer et al., 2019; Feofilov and Stuberrauch, 2019). Analyzing the Fig. 4, one can note the following: (1) the SR_{SR} histograms of CALIOP (Fig. 4a–e) are characterized by two distinct peaks corresponding to low-level and high-level clouds; this feature is coherent with other observations, e.g. with GEWEX (Global Energy and Water cycle Experiment) cloud assessment (Stuberrauch et al., 2013); (2) the SR_{ALADIN} histograms built for SRs retrieved from ALADIN's observations (Fig. 4f–j) are characterized by a smoother occurrence frequency plot where the two-peak structure is less pronounced than for CALIOP; (3) even though ALADIN detects some clouds in polar stratosphere (PSCs), **its overall sensitivity to high clouds ($>7\text{ km}$) is lower than that of CALIOP**. **(4) both rows show certain consistency of zone-to-zone change up to $\sim 3\text{ km}$ altitude while the behavior above requires a more detailed view.** **We would like to stress here that no linear scaling applied uniformly to SRs at all heights could change the ratio of high cloud detection frequency to low cloud detection frequency of ALADIN.** The same is true for CALIOP. In the next step, we compare the “instantaneous” profiles provided by CALIOP and ALADIN having in mind the peculiarities of cloud detection sensitivity differences observed in Fig. 4

3.2 Comparing pseudo-individual profiles at ALADIN's L2A product resolution

To address the high cloud detection sensitivity, we have inspected the 6h nighttime subset of collocated data, looking for the cases, which would satisfy the following criteria: (1) both instruments should have at least one strong SR peak; (2) the vertical position of this peak detected by one instrument should match that of the peak detected by a **second instrument within 1 km**; (3) the CALIOP SR profile should have a secondary peak at or above 9 km (Fig. 5a–j). For the comparison purposes, the panels in Fig. 5 represent the individual profiles belonging to the same 5 zones as the panels of Fig. 4. **For the sake of simplicity, we compare the SR_{ALADIN} profiles recalculated to SR_{SR} , but we also show the source SR_{ALADIN} profiles for reference purposes.** Regarding the conversion using Eq. 1, the strong peaks selected this way demonstrate a qualitative agreement between the

Author: Subject: Comment on Text Date: 18.05.2021 15:14:57
 which products? SR or cloud product? Unclear

Author: Subject: Comment on Text Date: 18.05.2021 15:15:04
 phrasing

Author: Subject: Comment on Text Date: 18.05.2021 15:16:04
 phrasing

Author: Subject: Comment on Text Date: 18.05.2021 15:17:14
 maybe because your transformation of the SR is incorrect?

Author: Subject: Comment on Text Date: 18.05.2021 15:18:07
 if you know that, why have you done so?

Author: Subject: Comment on Text Date: 14.06.2021 09:07:46
 What is true for CALIOP?

Author: Subject: Comment on Text Date: 14.06.2021 11:09:47
 is the feasible according to the range-bin setting of Aeolus. In principle, Aeolus can also have 2 km thick range bins. Can you comment on this?

Author: Subject: Comment on Text Date: 14.06.2021 10:08:26
 I do not see a reason to use the “sake of simplicity” here. A correct conversion is needed

AC: now we specify that we compare $SR(532\text{nm},z)$ and $SR(532\text{nm},z)$

AC: we have changed the phrasing

AC: Indeed, the updated transformation of SR gives somewhat better results, but the general conclusions (and the one, which is marked by the Reviewer on this page) remain the same

AC: please, see our answer regarding linear conversion in the text portion of the replies above

AC: That's true, 2km range bins can exist in ALADIN data, but they were not the subject of a case study described here (and we did not see them). As for the averaged plot, they will not spoil the picture, either, because the data is interpolated to a regular grid and then averaged.

AC: We do not use SR_{355} anymore and we apply an updated (and presumably correct) conversion procedure.

Author:	Subject: Comment on Text	Date: 14 06 2021 10:09:39
	This is not convincing	
Author:	Subject: Comment on Text	Date: 14 06 2021 10:10:13
	how do you account for the different vertical resolution?	
Author:	Subject: Comment on Text	Date: 14 06 2021 10:11:10
	This statement is not clear for me	
Author:	Subject: Comment on Text	Date: 14 06 2021 10:14:44
	Phrasing needs to be improved	

peak values calculated from SR_{335} and peak retrieved SR_{335} values in Appendix A, we demonstrate the correlation between individual pairs of CALIOP and ALADIN SR profiles; the comparison of this exercise is that it uses cases using Eq. 1, but the uncertainties of the analysis do not allow to retrieve conversion coefficients. As for the potential capability of ALADIN to detect high clouds, the subset Fig. 5a-e represents the cases, for which the instrument was capable of retrieving the peak of the same magnitude and height as the peak detected by CALIOP. Even though these cases exist, they are far less frequent than those shown in Fig. 5f-j. We did not detect and correlation between the collocation criteria ($\Delta dist$, $\Delta time$) and the frequency of occurrence of these cases, it's just a statistical observation that both types of cases exist and the former are less frequent than the latter. This observation gives a hint that the instrumental part provides the backscatter information sufficient for some cloud detection up to 20 km, but the detection algorithm suppresses noisy solutions. The PSC detection discussed below (see also Fig. 4f) confirms this assumption because the vertical extent and the composition of these clouds yield a strong signal. Further speculations on this subject are beyond the scope of the present article, but we believe that the high cloud detection agreement might be improved by studying the collocated cases provided in the supplementary materials and by applying different noise filtering techniques in the L0→L1→L2 elements of the ALADIN retrieval chain. Figures 5k-o will be discussed below in the context of low-level cloud observations.

3.3 Cloud detection agreement

To illustrate the peculiarities of zonal and altitudinal behavior of cloud detection agreement between two considered instruments, we have split the collocated data into four groups (Fig. 6). For each altitude/latitude grid point, we have estimated the number of cases when both instruments have detected a cloud ($SR_{335}(z) > 0$), when neither of instruments has detected a cloud, when only CALIOP has detected a cloud, and when only ALADIN has detected a cloud. For the sake of simplicity, we will call them YES_YES, NO_NO, YES_NO, and NO_YES cases. It is clear that in the ideal experiment the number of mismatched cases (YES_NO and NO_YES) should tend to zero. From the study presented in Section 2.4, we expect that the ratio of (YES_YES+NO_NO)/(YES_YES+NO_NO+YES_NO+NO_YES) should be about 0.77±0.17 if both instruments detect the clouds with the same efficiency. In Fig. 6a we show the ratio of YES_YES cases to the total number of collocated profiles per altitude/latitude bin. This panel resembles a typical cloud amount plot, and this is expected because in the case of an ideal agreement the aforementioned ratio is equivalent to cloud amount definition. Below, we will also discuss the YES_YES statistics normalized to cloud amount, but at this point we also want to study the other cases, which cannot be normalized this way. Even though the distribution in Fig. 6a looks physical, the absolute numbers are somewhat low and this is explained by YES_NO and NO_YES distributions (Fig. 6c and d, respectively). As for NO_NO agreement (Fig. 6b), it is close to 100% in the high-altitude area where there are no clouds. This indicates that the noise-induced false detection rate of both instruments is low, and this is a good sign.

If we consider the mismatch of YES_NO type (Fig. 6c), we will see that the altitudinal/zonal distribution of the mismatch occurrence frequency resembles that of the YES_YES type. A part of mismatch can be explained by theoretically allowed cloud detection disagreement discussed in Section 2.4. However, the occurrence frequency of YES_NO cases above 3 km is

AC: We do not have Appendix A and the corresponding discussion in the present version of the manuscript.

AC: When the profiles are compared, the resolution of CALIOP is already lowered through averaging.

AC: We've added an explanation after this phrase

AC: This section has been rewritten

Author: Subject: Comment on Text Date: 14.06.2021 10:17:13
 What does it mean? It could be also a cause of your rough conversion of the scattering ratio and or the range-bin thickness of Aeolus?

Author: Subject: Comment on Text Date: 14.06.2021 10:18:28
 Phrasing! Is this really only one cloud?

Author: Subject: Comment on Text Date: 14.06.2021 10:19:55
 Can you explain, how these false peaks could develop? It is not clear to me

roughly twice that of YES_YES cases, and this indicates the retrieval sensitivity issue of ALADIN. The NO_YES mismatches (Fig. 6d) require specific attention because they are not expected from the methodological point of view. The cloud extinction at 355 nm is larger than at 532 nm and the observation geometry of ALADIN makes the optical paths $1 / \cos(SZA) = 1.22$ times longer than those for CALIOP, where SVA stands for satellite viewing angle of 55°. The typical individual profiles corresponding to NO_YES mismatches are shown in Fig. 5k-o. As one can see, despite the unfavorable observation conditions (e.g. an opaque cloud with peak $SR_{0.5}$ value of ~22 at 9 km in Fig. 5l), ALADIN reports two valid points beneath the cloud, whereas it does not report anything at 9 km height where CALIOP sees a thick cloud. These cases do need our special attention. On the one hand, many cases of this type are over the ocean, so one can rule out the surface echo mixed with atmospheric backscatter and treated like an atmospheric signal. On the other hand, the NO_YES cases are often accompanied by the structures similar to those presented in Fig. 5k,l,n which are probably provoked by a presence of a cloud at these heights. The perturbations to the extinction and backscatter profile caused by these structures might propagate downwards, thus causing the appearance of the false peaks in the lower layers of ALADIN's data. This indicates a need for a quality flag refinement in the lower layers in the presence of a thick cloud above and the improvement of thick cloud detection itself. Apparently, the CALIOP cloud retrievals beneath thick clouds do not suffer from these effects.

To test whether the aforementioned disagreements are at least partially caused by the cloud definition and SR recalculation to another wavelength and whether the agreement could be improved, we varied the SR threshold for ALADIN, assuming the ±50% uncertainty on the parameters forming the coefficients of Eq. 1. However, this exercise yielded no optimum value for SR threshold: its lowering for ALADIN increased the number of YES_YES and reduced the number of YES_NO cases, but at the same time it increased the frequency of NO_YES cases. Correspondingly, increasing the threshold reduced the number of NO_YES cases, but it adversely affected the YES_YES agreement. Summarizing this comparison, one can conclude that (a) a cloud detected by CALIOP is detected by ALADIN in ~50% of cases for clouds below ~3 km and in ~30% of cases for higher clouds; (b) in the cloud-free area, the agreement between the datasets is good that indicates a low frequency of false positive detections by both instruments; (c) one half of the cases when ALADIN detects a cloud missed by CALIOP should be attributed to false positive detection of the low cloud in the presence of a higher opaque cloud, which perturbs the retrieval in the lower layers.

3.4 Cloud altitude detection sensitivity

Besides marking the profile elements as “cloudy” and “not cloudy” and comparing the cloud detection statistics as we did in the previous section, it would be interesting to obtain cloud peak detection statistics for pairs of collocated profiles like those shown in Fig. 5. This exercise is not aimed at revealing any altitude offset in backscatter signal registration, because this part of experimental setup is robust in both instruments. But, as we saw in Fig. 4 and Fig. 6, the sensitivity of ALADIN to high clouds is lower than to lower clouds and a convolution of sensitivity curve with the backscatter profile can skew the cloud peak position and the average cloud height. To illustrate this effect, we have carried out the following analysis. For each pair

AC: as we wrote before, the updated conversion algorithm did not change the magnitude of SRs for high clouds. In any case, the agreement of the updated version is somewhat better, so we changed the phrasing.

AC: this time, we consider all possible reasons for NO_YES cases, including those related to recalculation procedure. Our conclusion is that even if we tweak the conversion parameters, we will explain only half of these cases

AC: We do not know the exact details of the algorithms, so we can only speculate here using the basics of active remote sensing. Since the lidar equation (Eq. 1) is solved layer per layer and the upper layers affect the solution for the lower ones, the “false peaks” we were speaking about, can appear if the solution in the upper layer is perturbed by noise. We have added the explanations and toned down the phrasing of this section.

AC: yes, we meant the altitude, thanks

AC: fixed, thanks



of collocated profiles selected for YES_YES plot (Fig. 6a), we scanned through ALADIN profile step by step, looking for a local maximum, which we define as a set of the following conditions:

$$SR(i) > SR_{\text{threshold}}; \quad SR(i) > SR(i-1); \quad SR(i) > SR(i+1) \quad (2)$$

where $SR_{\text{threshold}}$ is the cloud detection threshold at 532 nm, which is equal to 5. For each local peak found, we have searched for a peak or for a maximal value of CALIOP's SR profile in the vicinity of **3.3 km** from the peak height determined from ALADIN. The choice of a "reference" dataset in this case depends on the detection probability, and if one chooses CALIOP as a reference, the distance to the nearest ALADIN peak might be spoiled by lower probability of cloud detection by ALADIN and the distribution will be skewed. The search limits are arbitrary and they have been chosen from inspecting the collocated profiles taking into account the natural variability of cloud heights at distances of about 100 km, estimated from the analysis of CALIOP data used in this study (~75% of clouds move vertically by less than 1 km, ~8% by 1–2 km, ~5% by 2–3 km, ~4% by 3–4 km, ~3% by 4–5 km and ~5% by more than 5 km). The differences between the ALADIN's and CALIOP's cloud peak heights have been stored and then averaged in the corresponding latitude/altitude bins (Fig. 7). As one can see, the cloud height detection agreement is better than 0.2 km below ~3 km and, surprisingly, for some of high-altitude zones. For the tropical zone, this is probably linked with thick Ci clouds which should be reliably detected by both instruments. For the Southern polar zone, this figure reveals the PSCs, which are barely visible in Fig. 6a, but which can be seen in Fig. 4f for ALADIN. These clouds form at very low temperatures and are composed of ice particles yielding a reflection, which is reliably detected at both wavelengths if the layer is thick (e.g. Adriani et al., 2004; Snels et al., 2021). As for the clouds between ~3 km and ~10 km height, the height sensitivity effects skew the effective cloud height detected by ALADIN downwards by 0.5–1.0 km. This is coherent with Fig. 4, which shows lower frequency of occurrence of high clouds detected by ALADIN. At least a part of the cloud peak shifts in the 3–5 km layer should be attributed to the reasons discussed for NO_YES statistics and these differences should reduce when the aforementioned quality flags for cloud-perturbed retrievals are fixed.

3.5 Temporal evolution of cloud detection agreement

ALADIN is a relatively young instrument and its calibration/validation activity is still on the way (Baars et al., 2020; Donovan et al., 2020; Kanitz et al., 2020; Rejebouch et al., 2020; Straume et al., 2020). This includes, but is not limited to internal calibration and comparisons with other observations. The Aeolus mission faced a number of technical issues, which hindered obtaining the planned specifications. These issues are related to several factors: (a) laser power degradation (60 mJ/pulse instead of 80 mJ/pulse) and signal losses in the emission and reception paths (33%) that results in lower signal to noise ratio (SNR) than planned, (b) telescope mirror temperature effects biasing the wind detection and calibration of Mie and Rayleigh channels of ALADIN, (c) constantly increasing number of hot pixels of both ACCD detectors (Weiler et al., 2021) leading to errors both in wind speed and in retrieved optical parameters of the atmosphere (the number of hot pixels increased by a factor of 1.4 during the period considered in this work). The Aeolus teams managed to mitigate some of these adverse effects (e.g. Baars et al., 2020; Weiler et al., 2021), and it would be interesting to see whether the pilot L2A dataset, Prototype_v3 10 is



free of cloud detection quality trends. If true, this would indicate a good calibration and consistent processing of Level 0 through Level 1 to Level 2A.

In Fig 8 and 9 we show the temporal evolution of cloud detection agreement per height bins. The panels of Fig 8 are consistent with those of Fig 6 whereas Fig 9 considers only the evolution of YES_YES statistics, which corresponds to Fig 6a and Fig 8a, normalized by cloud amount. Unfortunately, the period available for analysis does not cover the whole year, so the plots can be affected by seasonal variation of cloud distributions. Still, the latitudinal and longitudinal coverage of collocated data does not change throughout the year and a mixture of Northern and Southern hemispheres should partially compensate for seasonal anomalies. The signatures one should be looking for are experimental artefacts linked with laser power degradation, hot pixels appearance, and bias corrections. If these issues are not properly compensated, the “agreement panels” (Fig 8a, b) should demonstrate a decrease in occurrence frequency with time and the occurrence frequency in “disagreement panels” (Fig 8c, d) should increase with time. As one can see, this is not the case: visually, all 4 panels of Fig 8 do not show any anomaly, which would go beyond their noise levels (a special region corresponding to a forced bin size reduction in the period of 28/10/2019–10/11/2019 is marked by white dashed lines in Fig 8 and should not be considered at heights below 2250m). To quantify the tendencies and to compare them with noise levels, we have normalized Fig 8a (YES_YES cases) by cloud amount per altitude/time bin. This procedure helps to get rid of seasonal variation of clouds. The results presented in Fig 9 confirm the previous conclusions regarding the altitude distribution of cloud detection agreement: for the clouds below 3 km it is better than for higher ones ($61\pm 16\%$ and $34\pm 18\%$ for 0–75 and 75–225 km, respectively versus $24\pm 10\%$, $26\pm 10\%$, and $22\pm 12\%$ for 6–75 km, 75–1025 km, and 1025–225 km, respectively). As for the tendencies, the low-level clouds demonstrate an improvement towards the end of the year whereas the agreement for 6–75 km and 10–25 km becomes slightly worse by the end of the considered period.

If we compare the hot pixels distribution for Mie and Rayleigh channel ACCD detectors at the beginning and at the end of the time scale of Fig 8 and 9 (Table 2 of Weiler et al., 2021), we will see 3 and 5 new hot pixels for Mie and Rayleigh matrices, respectively. Even though the Rayleigh matrix pixels are not directly linked to cloud detection, their information is used for the ALADIN SR calculations. For Mie matrix, the lowermost hot pixel, which appeared during the considered period, corresponds to ~15 km height and this cannot affect the tendencies shown in Fig 9. As for new Rayleigh hot pixels, the lowermost two corresponds to 1 km height, the next two – to 5 km height, and the last one – to 18 km. This information does not explain the observed behavior, either. Overall, considering relatively large error bars for all five altitudinal sections presented in Fig 9b and the variety of the observed slopes, one cannot make a sound conclusion neither regarding the deterioration (or the improvement) of cloud detection agreement nor regarding the link between hot pixels appearance and change of cloud detection quality. A proper conclusion is that one does not detect the tendencies beyond the variability limits of the analyzed parameter and that the hot pixels appearance cannot be tracked from the cloud agreement plot, indicating that compensation for hot pixels effects (Weiler et al., 2021) works properly within the discussed uncertainty limits. The same can be said regarding the other known technical issues: the signal losses in the emission and reception paths do not transform into



a clear signature in cloud detection agreement plots. Moreover, they should have affected the detection of low and high clouds in the same way that is not observed in Fig. 8 and 9

4. Conclusions

The active sounders are advantageous for atmospheric and climate studies because they provide atmospheric parameters at altitude resolved scale with high accuracy. For continuity of climate studies and monitoring the global changes it is essential to understand the differences between spaceborne lidars operating at different wavelengths, flying at different orbits, and utilizing different observation geometries, receiving paths, and detectors. In this article, we addressed an intercomparison of ALADIN and CALIOP lidars using their scattering ratio products (CALIPSO-GOCCP and Aeolus L2A, Prototype v3.10) for the period of 28/06/2019–31/12/2019.

Using the COSP2 lidar simulator coupled with output from the EAMv1 model and a horizontal cloud variability parameterization, we estimated a theoretically achievable agreement in cloud detection of 0.77 ± 0.17 for these two instruments with their orbits, averaging, and observation geometry.

On the one hand, the spatial collocation criterion of 1° chosen in this work is based on averaging distance of Aeolus L2A Prototype v3.10 data. On the other hand, the temporal collocation criterion of $\Delta t_{\text{time}} < 6\text{ h}$ is a tradeoff between the geographical coverage of the collocated profiles, their number, and uniformity of Δt_{time} distribution throughout the globe. With the named criteria, we managed to find $\sim 7.8\text{E}4$ collocated nighttime profiles, which underwent a series of analysis summarized here. For the simplicity of the comparison with CALIOP, we converted SR_{ALADIN} to SR_{CALIOP} and we discuss the sensitivity of the results to the conversion parameters.

Overall, the SR product of ALADIN is characterized by lower sensitivity to high clouds above $\sim 7\text{ km}$ than CALIOP, that we explain by lower SNR for ALADIN at these heights that is due both to physical reasons (smaller backscatter at 355 nm) and technical reasons (hot pixels, lower emission and lower transmissivity of receive path than planned). Large sensitivity to lower

clouds leads to prioritizing the lower cloud solutions to higher ones in the case of a continuous cloud or a double layer. This skews the ALADIN's cloud peak height in pairs of ALADIN/CALIOP profiles by $\sim 0.5 \pm 0.4\text{ km}$ downwards. Interestingly, the agreement of PSC peak heights does not suffer from these effects. We explain this by large vertical extent and composition of PSCs, which make them a better target for ALADIN than the tropospheric clouds. In the cloud-free area, the agreement between two instruments is good indicating low rate of noise-induced false detection for both instruments. Last, but not least, the temporal evolution of cloud agreement does not reveal any statistically significant change during the considered period. This indicates that hot pixels and laser energy and receiving path degradation effects in ALADIN have been mitigated at least down to the uncertainties of the following cloud detection agreement values: $61 \pm 16\%$, $34 \pm 18\%$, $24 \pm 10\%$, $26 \pm 10\%$, and $22 \pm 12\%$ estimated at 0.75 km , 2.25 km , 6.75 km , 8.75 km , and 10.25 km , respectively. We believe that the provided collocated dataset will facilitate the further analysis and improvement of ALADIN L2A data.

Page: 12

Author: Subject: Comment on Text Date: 14.06.2021 10:28:59
why should there be a smaller backscatter at 355? This is in absolute contradiction to all my knowledge? Particle backscatter coefficient could be equal (Angström 0), Molecular backscatter coefficient is for sure higher and thus total backscatter is for sure also higher!

Author: Subject: Comment on Text Date: 14.06.2021 10:30:01
phrasing poor

AC: please, see our comment in the text section. What was meant was the "information content" of particulate backscatter with its noise with respect to molecular one, not the signal itself. Please, apologize for the confusion.

AC: we have rewritten this section



Appendix A

The analysis of the collocated data may enable the researcher not only to validate one dataset against another one, but also to validate a physical concept or to retrieve an important model parameter (e.g. Holl et al., 2010; Feofilov and Petelin, 2010; Feofilov et al., 2012; Viranen et al., 2018). In this section, we report the results of a validation attempt aimed at the retrieval of the scaling coefficients used in Eq. 1 and through them the model assumptions. To do this, we searched the collocated database for the events which would satisfy the following criteria: (a) the ALADIN SR profile should contain at least one valid point with the corresponding quality flags (see Section 2.2) and with SR higher than halved $SR_{threshold}$; (b) the profiles should fit the selection criteria used for cloud altitude detection sensitivity (Section 3.4); (c) the CALIOP peak should contain more than one point to avoid sampling problems. For these profiles, we picked up not only the major peak values, but also the secondary peak values if the vertical agreement of the profiles was good like in Fig. 3a,c,d,e. The corresponding pairs of SR_{CALIOP} and SR_{ALADIN} values have been binned using the 0.2×0.07 SR bins, which reflect the differences between SR_{SR2} and SR_{SR3} . The corresponding frequency occurrence distribution for this dataset is shown in Fig. A1. Even though the SR pairs exist for opaque domain, the spread increases and the values beyond $SR_{SR3} = 10$ are neither informative nor suitable for the maximal probability search algorithm (see Dawkins et al., 2018) used for the analysis. Like in Fig. 11 of (Dawkins et al., 2018), the red dots in Fig. A1 represent the centers of Gaussian fit to perpendicular transects. White dashed line shows a linear fit to the dataset represented by these red dots, and the corresponding conversion is given by the following equation:

$$SR_{SR2} = SR_{SR3} \times (3.8 \pm 1.0) - (3.3 \pm 1.4) \quad (A1)$$

Even though the coefficients in Eq. A1 differ from those of Eq. 1, the black dashed line in Fig. A1 representing Eq. 1 does not significantly deviate from the white dashed line representing Eq. A1 and both lines fit the maximum probability plot within its uncertainty limits. We conclude that the collocated dataset proves the basic equations used to derive Eq. 1 though its uncertainties do not allow to retrieve the corresponding fitting parameter Λ of (Collis and Russell, 1976) from such a comparison.

<https://doi.org/10.5194/amt-2021-96>
Preprint. Discussion started: 19 April 2021
© Author(s) 2021. CC BY 4.0 License.



Data availability

The collocated dataset used in this work can be downloaded from ResearchGate repository using the following link
<https://doi.org/10.13140/RG.2.2.11237.12009> (Feofilov et al., 2021)

Author contribution

410 HC, VN, MC, and AF: conceptualization, investigation, methodology, and validation; RG, CG, and AF: data curation and formal analysis; AF: writing original draft; AF and HC: review and editing

Competing interests

The authors declare that they have no conflict of interest

Disclaimer

415 The presented work includes preliminary data (not fully calibrated/validated and not yet publicly released) of the Aeolus mission that is part of the European Space Agency (ESA) Earth Explorer Program. This includes aerosol and cloud products, which have not yet been publicly released. Aerosol and cloud products will become publicly available by spring 2021. The processor development, improvement and product preprocessing preparation are performed by the Aeolus DISC (Data, Innovation and Science Cluster), which involves DLR, DoRIT, ECMWF, KNMI, CNRS, S&T, ABB and Serco, in close cooperation with the Aeolus PDGS (Payload Data Ground Segment)

Acknowledgements

This work is supported by the Centre National de la Recherche Scientifique (CNRS) and by the Centre National d'Etudes Spatiales (CNES) through the Expecting Earth-Care, Learning from A-Train (EECLAT) project. The processor development, improvement and product preprocessing preparation are performed by the Aeolus DISC (Data, Innovation and Science Cluster), which involves DLR, DoRIT, ECMWF, KNMI, CNRS, S&T, ABB and Serco, in close cooperation with the Aeolus PDGS (Payload Data Ground Segment). The authors want to thank P.-L. Ma (PNNL) for providing the outputs of the EAMv1 atmospheric model and F. Ehlers (EOP-SMA/ESTEC/ESA), A. Straume (ESTEC/ESA), and O. Reiterbuch (DLR) for their comments on the preliminary version of the manuscript



AC: This is true, but this is the only source of information available. A comment from a Technical Editor is needed for such a case.

430 References

- ADM-Aeolus Science Report, SP-1311, ISBN 978-92-9221-404-3, ISSN 0379-6566, Co-ordinated by: P. Ingmann, Mission Science Division, Atmospheric Unit, Published by: ESA Communication Production Office, The Netherlands, 121pp, 2008
- Adriani, A., Massoli, P., Di Donfrancesco, G., Cairo, F., Moriconi, M. I., Sneli, M.: Climatology of polar stratospheric clouds based on lidar observations from 1993 to 2001 over McMurdo Station, Antarctica, *J. Geophys. Res.*, 109, D24211, doi:10.1029/2004JD004800, 2004
- Ansmann, A., Wandinger, U., Le Rille, O., Lys, D., and Straume, A. G.: Particle backscatter and extinction profiling with the spaceborne high-spectral-resolution-Doppler lidar ALADIN: methodology and simulations. *Appl. Optics*, 46 (26), 6606–6622, doi:10.1364/AO.46.006606, 2007
- Baars, H., Geiß, A., Wandinger, U., Herzog, A., Engelmann, R., Bühl, J., Radenz, M., Seifert, P., Ansmann, A., Martin, A., Leinweber, P., Lehmann, V., Weismann, M., Cress, A., Filioglou, M., Komppula, M., and Reitebuch, O.: First Results from the German CalVal Activities for Aeolus, EPJ Web Conf. 237, 01008, doi:10.1051/epjconf/202023701008, 2020
- aley, S., IT Consulting Group B.V., Aeolus Atmospheric Sampling - Range Bin Settings, available at https://www.aeolus.esa.int/confidence/pages/viewpage.action?spaceKey=CALVAL&title=Vs+002_2021**
- Boutle, J. A., Abel, S. J., Hill, P. G., Morcrette, C. J.: Spatial variability of liquid cloud and rain: observations and microphysical effects, *Q. J. R. Meteorol. Soc.*, 140, 583–594, doi:10.1002/qj.2140, 2014
- Chunin, M. L., Garnier, A., Hauchecorne, A., and Porteneuve, J.: A Doppler lidar for measuring winds in the middle atmosphere, *Geophys. Res. Lett.* 16(11), 1273–1276, doi:10.1029/GL016011p01273, 1989
- Chahine, M. T. and 30 Coauthors: AIRS: Improving weather forecasting and providing new data on green-house gases, *Bull. Amer. Meteor. Soc.*, 87(7), 911–926, doi:10.1175/BAMS-87-7-911, 2006
- Chalon G., Cayla F. R., Diebel D.: IASI: An advance sounder for operational meteorology, Proc. 52nd Congress of IAF, Toulouse France, CNES, available online at http://smc.cnes.fr/documentation/IASI/Publications/PR_ESENTATION_IASI_2001.pdf, 2001
- Chepfer H., Bony, S., Winker, D., Chiriaco, M., Dufresne, J.-L., Séze, G.: Use of CALIPSO lidar observations to evaluate the cloudiness simulated by a climate model, *Geophys. Res. Lett.*, 35, L15704, doi:10.1029/2008GL034207, 2008
- Chepfer H., Bony, S., Winker, D., Cesana, G., Dufresne, J.-L., Minnis, P., Stubenrauch, C. J., and Zeng, S.: The GCM Oriented Calipso Cloud Product (CALIPSO-GOCCP), *J. Geophys. Res.*, 115, D00H16, doi:10.1029/2009JD012251, 2010
- Chepfer, H., Noel, V., Winker, D., and Chiriaco, M.: Where and when will we observe cloud changes due to climate warming?, *Geophys. Res. Lett.*, 41, 8387–8395, doi:10.1002/2014GL061792, 2014
- Chepfer H., Noel, V., Chiriaco, M., Wielicki, B., Winker, D., Loeb, N., and Wood, R.: The potential of multi-decades space-born lidar to constrain cloud feedbacks, *J. Geophys. Res. Atmos.*, DOI:10.1002/2017JD027742, 2018
- Chepfer, H., Brogniez, H., and Noel, V.: Diurnal variations of cloud and relative humidity profiles across the tropics, *Sci. Rep.*, 9, 16045, doi:10.1038/s41598-019-52437-6, 2019

<https://doi.org/10.5194/amt-2021-96>
 Preprint. Discussion started: 19 April 2021
 © Author(s) 2021. CC BY 4.0 License.



- Collis, R. T. H., Russell, P. B.: Lidar measurement of particles and gases by elastic backscattering and differential absorption, *Laser Monitoring of the Atmosphere*, Topics in Applied Physics, 14, ISBN 978-3-540-07743-5 Springer-Verlag, 71– 130, doi:10.1007/3-540-07743-X_18, 1976
- Dawkins, E. C. M., Feofilov, A., Rezac, L., Kutepov, A. A., Janches, D., Höffner, J., X. Chu, X., Lu, X., Mlynarczyk, M. G., and Russell III, J.: Validation of SABER v2 Operational temperature data with ground-based lidars in the mesosphere-lower thermosphere region (75–105 km), *J Geophys Res Atmos*, 123, 9916–9934, doi:10.1029/2018JD028742, 2018
- Donovan, D. P., Marselle, G.-J., de Kloe, J., and Stoffelen, A.: AEOLUS L2 activities at KNMI, EPJ Web Conf. 237, 01002, doi:10.1051/epjconf/20202370100, 2020
- Feofilov, A. G., Chepfer, H., Noel, V., Guzman, R., Gindre, C., and Chiriaco, M.: Colocated ALADIN/Aeolus and CALIOP/CALIPSO observations for the period of 28/06/2019–31/12/2019, *ResearchGate*, <https://doi.org/10.13140/RG.2.2.11237.12009>, 2021
- Feofilov, A. G. and Petelina, S. V.: Relation between mesospheric ice clouds, temperature, and water vapor determined from Odin/OSIRIS and TIMED/SABER data, *J Geophys Res*, 115, D18305, doi:10.1029/2009JD013619, 2010
- Feofilov, A. G., Kutepov, A. A., She, C.-Y., Smith, A. K., Penell, W. D., and Goldberg, R. A.: CO₂(v₂)-O quenching rate coefficient derived from coincidental SABER/TIMED and Fort Collins lidar observations of the mesosphere and lower thermosphere, *Atmos Chem Phys*, 12, 9013–9023, doi:10.5194/acp-12-9013-2012, 2012
- Feofilov, A. G. and Stuberrauch, C. J.: Diurnal variation of high-level clouds from the synergy of AIRS and IASI space-borne infrared sounders, *Atmos Chem Phys*, 19, 13957–13972, doi:10.5194/acp-19-13957-2019, 2019
- Guzman, R., Chepfer, H., Noel, V., Vaillant de Guelis, T., Kay, J. E., Rabaranto, P., Cesana, G., Vaughan, M. A., and Winker, D. M.: Direct atmosphere opacity observations from CALIPSO provide new constraints on cloud-radiation interactions, *J Geophys Res Atmos*, 122, 1066–1085, doi:10.1002/2016JD025946, 2017
- Hélière, A., Gelsdorpe, R., Le Hors, L., and Toulemon, Y.: ATLID, the Atmospheric Lidar on board the EarthCARE Satellite, *Proceedings of the ICSO (International Conference on Space Optics)*, Ajaccio, Corse, France, Oct. 9–12, 2012, paper: ICSO-065, 2012
- Hilton, F., and 42 Coauthors: Hyperspectral Earth observation from IASI: Five years of accomplishments, *Bull. Am. Meteorol. Soc.*, 93, 347–370, doi:10.1175/BAMS-D-11-00027.1, 2012
- Flamant, P., Cuesta, J., Denneulin, M.-L., Dabas, A., and Hubert, D.: ADM-Aeolus retrieval algorithms for aerosol and cloud products, *Tellus*, 60(2), 273–288, doi:10.1111/j.1600-0870.2007.00287.x, 2008
- Flamant, P. H., Lever, V., Martinet, P., Flamant, T., Cuesta, J., Dabas, A., Olivier, M., and Huber, D.: ADM-Aeolus L2A Algorithm Theoretical Baseline DocumentParticle spin-off products, AE-TN-IPSL-GS-001, V5.5, ESA, available online at <https://earth.esa.int/eogateway/documents/20142/0/Aeolus-L2A-Algorithm-Theoretical-Baseline-Documents-pdft.83pp>, 2017
- Holl, G., Buehler, S. A., Rydberg, B., and Jiménez, C.: Collocating satellite-based radar and radiometer measurements – methodology and usage examples, *Atmos. Meas. Tech.*, 3, 693–708, doi:10.5194/amt-3-693-2010, 2010

<https://doi.org/10.5194/amt-2021-96>
 Preprint. Discussion started: 19 April 2021
 © Author(s) 2021. CC BY 4.0 License.



- 500 Kamitz, T., and 24 Coauthors, ESA's Lidar Missions Aeolus and EarthCARE, EPJ Web Conf. 237, 01006,
doi:10.1051/epjconf/202023701006, 2020
- Krawczyk, R., Ghibaudo, J.-B., Labandibar, J.-Y., Willets, D. V., Vaughan, M., Pearson, G. N., Harris, M. R., Flamant, P.
H., Salamon, P., Dobas, A. M., Charasse, R., Royer, M., and Heinel, H.: ALADIN: an atmosphere laser
Doppler wind lidar instrument for wind velocity measurements from space, Proc. SPIE 2581, Lidar Techniques for Remote
Sensing II, (15 December 1995); doi:10.1117/12.228509, 1995
- Lolli, S., Delaval, A., Loth, C., Garnier, A., and Flamant, P. H.: 0.355-micrometer direct detection wind lidar under testing
during a field campaign in consideration of ESA's ADM-Aeolus mission, Atmos. Meas. Tech., 6, 3349–3358, doi:10.5194/amt-
6-3349-2013, 2013
- 505 Nam, C., Bony, S., Dufresne, J. L., Chepfer, H.: The 'too few, too bright' tropical low-cloud problem in CMIP5 models,
Geophys. Res. Lett., 39, 21, doi:10.1029/2012GL053421, 2012
- Noel, V., Chepfer, H., Chiriaco, M., and Yorks, J.: The diurnal cycle of cloud profiles over land and ocean between 51° S and
51° N, seen by the CATS spaceborne lidar from the International Space Station, Atmos. Chem. Phys., 18, 9457–9473,
doi:10.5194/acp-18-9457-2018, 2018
- 510 McGill, M. J., Yorks, J. E., Scott, V. S., Kupchuk, A. W., and Selmer, P. A.: The Cloud-Aerosol Transport System (CATS):
A technology demonstration on the International Space Station, Proc. SPIE, 9612, doi:10.1117/12.2190841, 2015
- Menzel, W. P., Frey, R. A., Borbas, E. E., Baum, B. A., Cureton, G., and Bearson, N.: Reprocessing of HIRS Satellite
Measurements from 1980 to 2015: Development towards a consistent decadal cloud record, J. Appl. Meteorol. Clim., 55,
2397–2410, doi:10.1175/JAMC-D-16-0129.1, 2016
- 515 Rasch, P., and 41 Coauthors: An Overview of the Atmospheric Component of the Energy Exascale Earth System Model, J.
Adv. Model. Earth Syst., 11, e2019MS001629, doi:10.1029/2019MS001629, 2019
- Reitebuch, O., and 27 Coauthors: Initial Assessment of the Performance of the First Wind Lidar in Space on Aeolus, EPJ Web
Conf. 237, 01010, doi:10.1051/epjconf/202023701010, 2020
- Reverdy, M., Chepfer, H., Donovan, D., Noel, V., Cesana, G., Horeau, C., Chiriaco, M., Bastin, S.: An EarthCARE/ATLID
simulator to evaluate cloud description in climate models, J. Geophys. Res. Atmos., 120(21), 11090–11113,
doi:10.1002/2015JD023919, 2015
- 520 Smith, W. L.: The TIROS-N operational vertical sounder, Bull. Am. Meteorol. Soc., 60, 1177–1187, 1979
- Snelis, M., Colao, F., Cairo, F., Shuli, I., Soccione, A., De Muro, M., Pitts, M., Poole, L., and Di Liberto, L.: Quasi-coincident
observations of polar stratospheric clouds by ground-based lidar and CALIOP at Concordia (Dome C, Antarctica) from 2014
to 2018, Atmos. Chem. Phys., 21, 2165–2178, doi:10.5194/acp-21-2165-2021, 2021
- Stephens, G. L., Hakuba, M. Z., Webb, M. J., Leeson, M., Yue, Q., Kahn, B. H., Hristova-Veleva, S., Rapp, A. D.,
Stubenrauch, C. J., Elsasser, G. S., and Slingo, J.: Regional Intensification of the Tropical Hydro-logical Cycle During ENSO,
Geophys. Res. Lett., 45, 4361–4370, doi:10.1029/2018GL077598, 2018

<https://doi.org/10.5194/amt-2021-96>
 Preprint. Discussion started: 19 April 2021
 © Author(s) 2021. CC BY 4.0 License.



- Stoffelen, A., Paillex, J., Källén, E., Vaughan, J. M., Isaksen, I., Flamant, P., Wergen, W., Andersson, E., Schyberg, H.,
 Culoma, A., Meynart, R., Endemann, M., and Ingmann, P.: The Atmospheric Dynamics Mission For Global Wind Field
 Measurement, *Bull Amer Meteor Soc*, 86, 73–87, doi:10.1175/BAMS-86-1-73, 2005
- Strueme, A. G. and 27 Coauthors: ESA's Space-Based Doppler Wind Lidar Mission Aeolus – First Wind and Aerosol Product
 Assessment Results, *EPJ Web Conf* 237, 01007, doi:10.1051/epjconf/20202370100, 2020
- Stubenrauch, C. J., and 22 Coauthors: Assessment of global cloud datasets from satellites: Project and database initiated by
 the GEWEX radiation panel, *Bull Am Meteorol Soc*, 94(7), 1031–1049, doi:10.1175/BAMS-D-12-00117.1, 2013
- Stubenrauch, C. J., Feofilov, A. G., Protopapadaki, S. E., and Armatte, R.: Cloud climatologies from the infrared sounders
 AIRS and IASI: strengths and applications, *Atmos Chem Phys*, 17, 13625–13644, doi:10.5194/acp-17-13625-
 2017, 2017
- Swales, D. J., Pincus, R., & Bodas-Salcedo, A.: The cloud feedback model intercomparison project observational simulator
 package, Version 2 Geoscientific Model Development, 11, 77–81, doi:10.5194/gmd-11-77-2018, 2018
- Vallant de Guelis, T. H., Chepfer, N., V. Guzman, R., Bonazzola, M., and Winker, D. M.: Space lidar observations constrain
 longwave cloud feedback, *Nature Sci Rep*, 8, 16570, doi:10.1038/s41598-018-34943-1, 2018
- Virtanen, T. H., Kolmonen, P., Sogacheva, L., Rodriguez, E., Saponaro, G., and de Leeuw, G.: Collocation mismatch
 uncertainties in satellite aerosol retrieval validation, *Atmos Meas Tech*, 11, 925–938, doi:10.5194/amt-11-925-2018, 2018
- Weiler, F., Kanitz, T., Wernham, D., Rennie, M., Huber, D., Schilling, M., Saint-Pe, O., Bell, R., Parniello, T., and
 Reibebuch, O.: Characterization of dark current signal measurements of the ACCDs used on-board the Aeolus satellite, *Atmos
 Meas Tech Discuss* [preprint], doi:10.5194/amt-2020-458, in review, 2020
- Winker, D. M., Vaughan, M. A., Omar, A. H., Hu, Y., Powell, K. A., Liu, Z., Hunt, W. H., and Young, S. A.: Overview of the
 CALIPSO Mission and CALIOP Data Processing Algorithms, *J Atmos Ocean Tech*, 26, 2310–2323,
 doi:10.1175/2009JTECHA1281.1, 2009

Instrument	Orbit inclination [deg]	Equator crossing LT [h]	Off-nadir angle [deg]	PRF [Hz]	Native resolution [deg]	L2 resolution resolution [deg]
ALADIN	96.97	6:00 / 18:00	35	30.0	140 (H) x 1000 (V)	87000 (H) x 1000 (V)
CALIOP	98.00	01:30 / 13:30	3	20.1	333 (H) x 60 (V)	333 (H) x 500 (V)

Table 1: Comparison of orbital parameters, viewing geometries, and resolutions of ALADIN and CALIOP instruments

Δt_{time} [h]	Daytime $\times 1E3$	Night-time $\times 1E3$	Total $\times 1E3$	Remarks
< 1	4.3	3.7	8	Narrow polar zone
< 3	13.1	11.2	24.3	Broader polar zone
< 6	91	78	169	All zones covered
< 12	135	116	251	Unequal distribution of Δt_{time}
< 24	176	146	322	Unequal distribution of Δt_{time}

Table 2: Number of collocated cases for $\Delta \text{dist} < 1^\circ$ and different Δt_{time} values

AC: Fixed, thanks

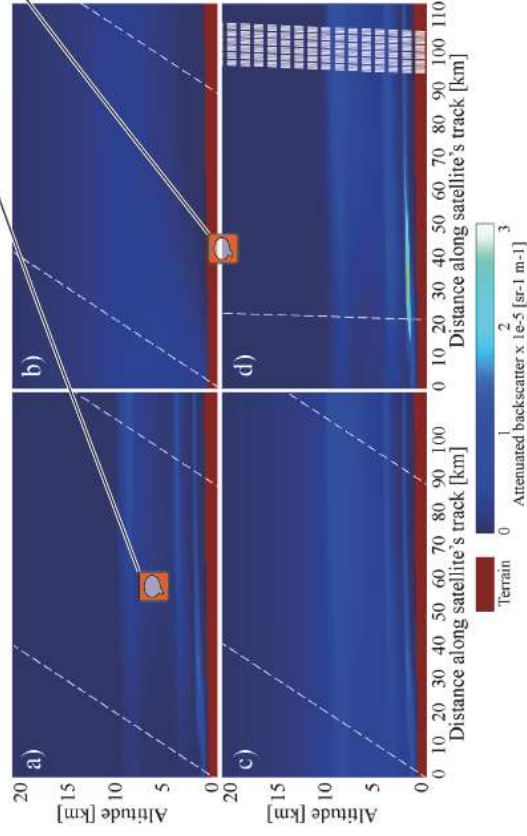


Figure 1: Observation geometry, averaging, and retrieved parameters for (a-c) ALADIN/Aeolus at its L2A resolution of 87 km and (d) CALIOP/CALIPSO at its native resolution: (a) Attenuated particular backscatter (APB) at 355 nm; (b) Attenuated molecular backscatter (AMB) at 355 nm; (c) Attenuated total backscatter (ATB) at 355 nm; (d) Attenuated total backscatter (ATB) at 532 nm. The scene has been calculated for demonstration purposes using COSP2 simulations with the EAMV1 model data as an input. White dashed lines stand in (a-c) for ALADIN's observation paths for centers of averaged profiles and in (d) for CALIOP averaged observation path corresponding to averaged ALADIN on the left and for individual CALIOP profiles on the right (with its 3° off-nadir viewing angle). ALADIN observes the atmosphere at 35° to the nadir and perpendicular to the flight direction. This inclination is schematically shown as an inclined line lying in lidar curtain plane whereas the real projection to the same plane should be a vertical line.

AC: Fig. 1 has been replaced with a 3D orbital view. The explanation of the numerical experiment refers more to a flowchart in Fig. 3

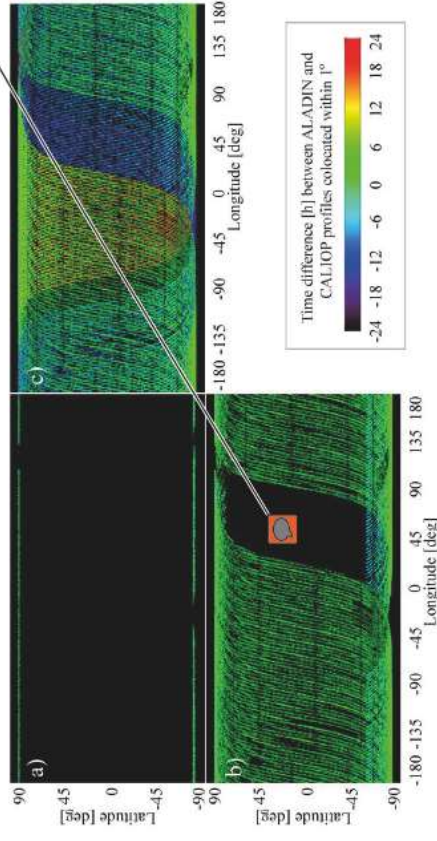
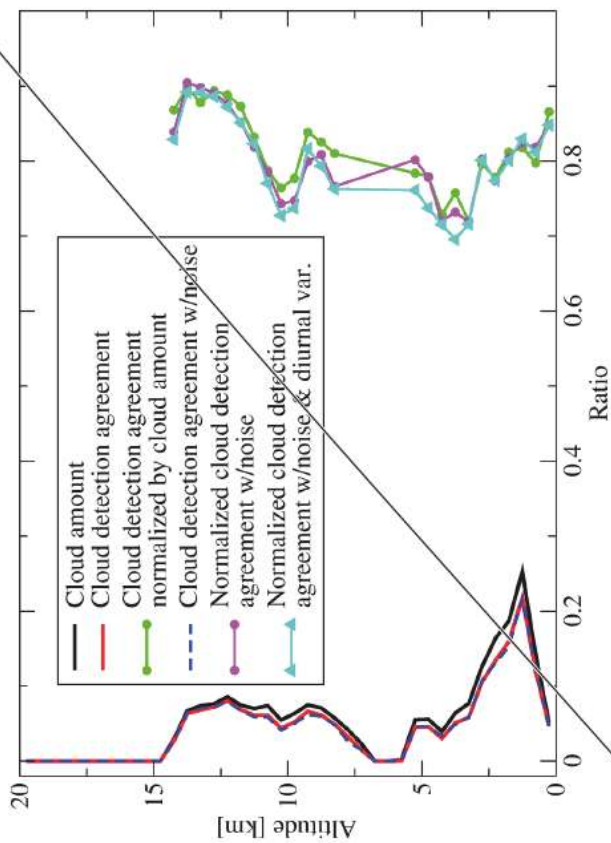


Figure 2: Geographical distribution of collocated points for (a) $\Delta\text{time} < 1\text{ h}$; (b) $\Delta\text{time} < 6\text{ h}$; (c) $\Delta\text{time} < 24\text{ h}$ for $\text{Adist} < 1^\circ$.

AC: this is a good question - due to large overhead at the collocation, we did not read the previous or next day. As a result, the collocation algorithm did not find anything for the data measured, for example, 4h earlier at a given longitude. In the present version, this figure has been replaced with 2D histograms in the latitudinal bins, but the gap remains in the collocated dataset.

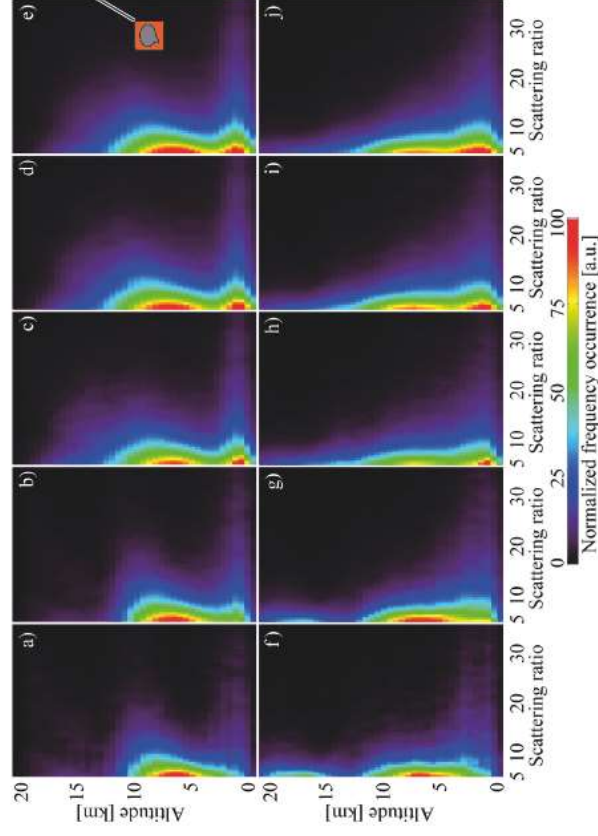
AC: we have updated the figure caption

570



575

AC: we tried white background, but it didn't improve the image. Instead, we zoomed in and moved the left-hand-side limit to $SR=3$ to show more of small SR values. We believe, this made the figure more informative.



580 Figure 4: Zonal mean comparison for the Atmos < 6h, Adist < 1° collected nighttime data subset (see Table 2): (a)-(e) CALIOP
averages; (f)-(h) ALADIN averages, converted to SR at 532 nm for comparison purposes; (a,e) 90S-60S; (b,f) 60S-30S; (c,h) 30S-
30N; (d,f) 30N-60N; (g,h) 60N-90N.

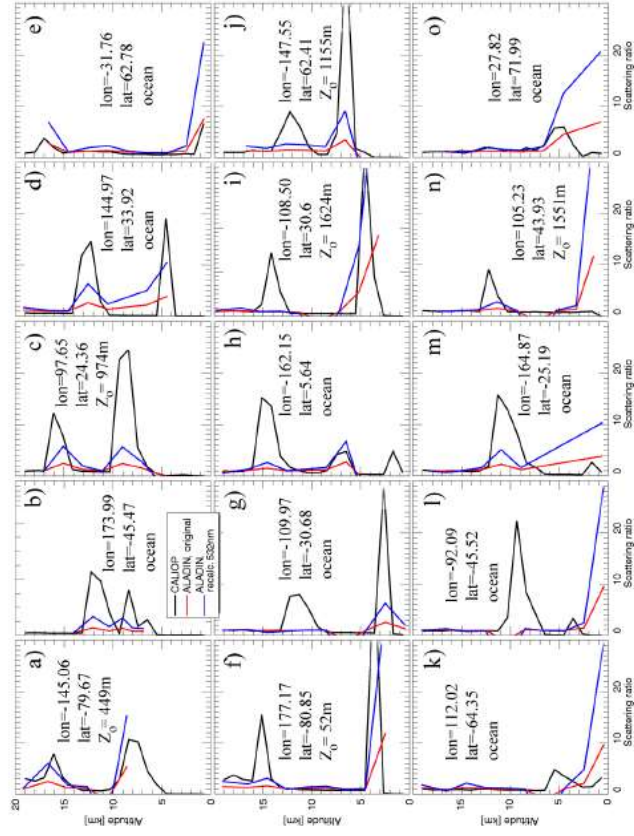
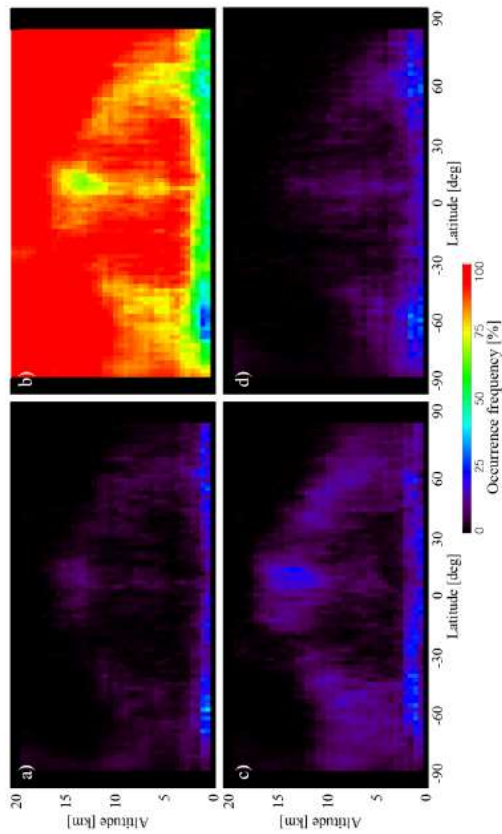


Figure 5: Pseudo-instantaneous comparison of collocated ALADIN L2A SR profiles and CALIOP SR profiles averaged over 67 km along the track: (a, f, k) 90S-60S; (b, g, l) 60S-30S; (c, h, m) 30S-30N; (d, i, n) 30N-60N; (e, j, o) 60N-90N; (a-e) cases confirming ALADIN's capability to detect high-level clouds; (f-j) cases showing the cases when ALADIN misses a high cloud detected by CALIOP; (k-n) cases explaining the presumably false detection of a low level cloud by ALADIN; (o) a case with a real low cloud detected by both instruments with an extra point near the surface reported by ALADIN.

<https://doi.org/10.5194/amt-2021-96>
Preprint. Discussion started: 19 April 2021
© Author(s) 2021. CC BY 4.0 License.



590 **Figure 6:** Cloud detection agreement: a) both CALIOP and ALADIN have detected a cloud (YES/YES case); b) neither CALIOP nor ALADIN has detected a cloud (NO/NO case); c) CALIOP has detected a cloud whereas ALADIN has not detected a cloud (YES/NO case); d) CALIOP does not detect a cloud whereas ALADIN has detected a cloud (NO/YES case).

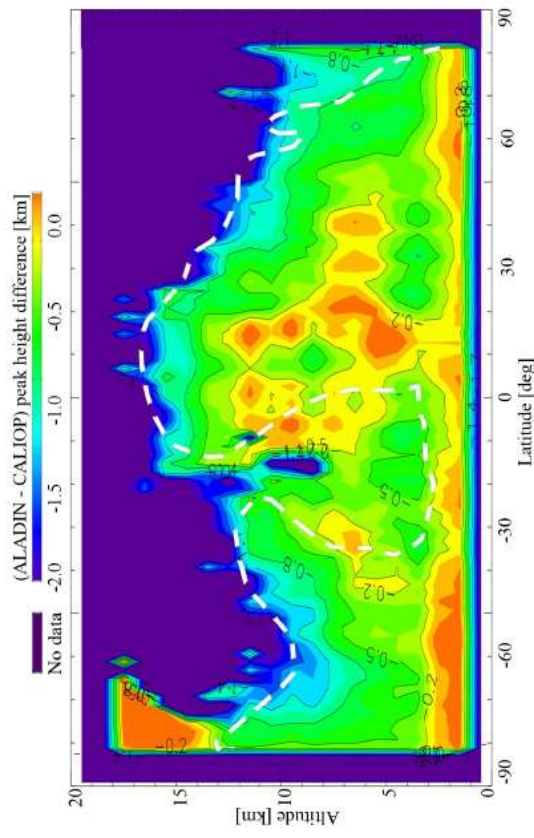


Figure 7: Cloud altitude detection sensitivity represented as a height difference between the CALIOP local peak height and corresponding ALADIN's cloud peak height or maximal SR height found in the ± 3 km vicinity of CALIPSO peak. The subset corresponding to YES_YES selection (Fig. 6a) was used. White dashed isoline corresponds to colored area in Fig. 6a (occurrence frequency of about 5% and higher).

<https://doi.org/10.5194/amt-2021-96>
 Preprint. Discussion started: 19 April 2021
 © Author(s) 2021. CC BY 4.0 License.

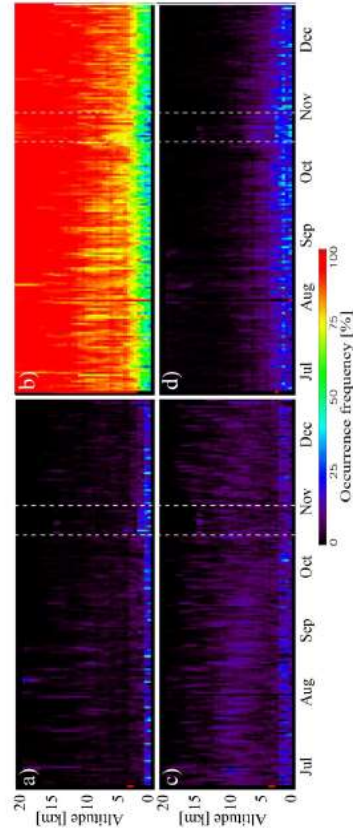


Figure 8: Temporal evolution of cloud detection agreement for the period of 28/06/2019–31/12/2019. The legend is consistent with that of Fig. 6: a) YES/YES; b) NO/NO; c) YES/NO; d) NO/YES. White vertical dashed lines correspond to the period of Air Motion Vector (AMV) campaign (28/10/2019–10/11/2019), which is characterized by smaller bin sizes and, therefore, larger SNRs for Mie and Rayleigh channels up to the height of 2250m.

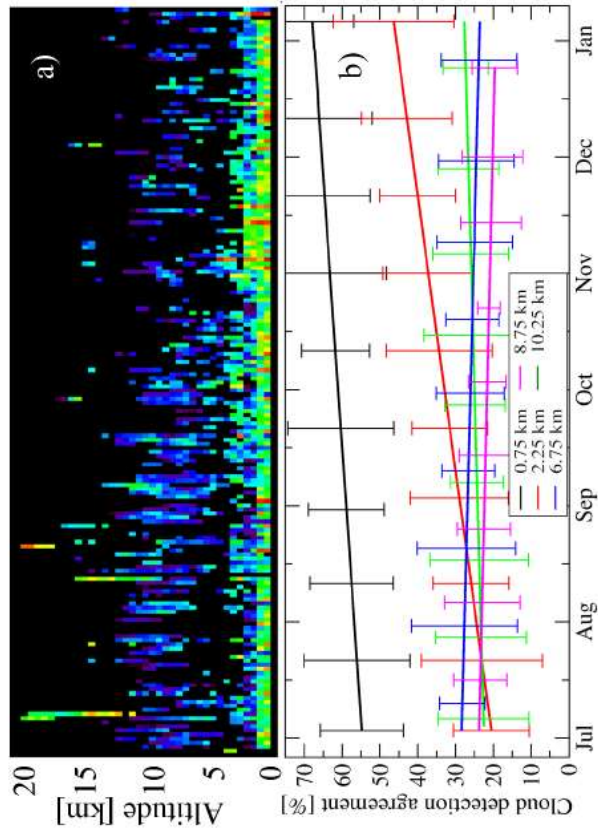


Figure 9: Temporal evolution of normalized cloud detection agreement for the period of 28/06/2019-31/12/2019; a) YES, YES statistics of Fig. 8a, normalized by cloud amount; b) the same information presented for 5 heights as linear fits in 2D with error bars. The color scheme for panel (a) is consistent with that of Fig. 8.

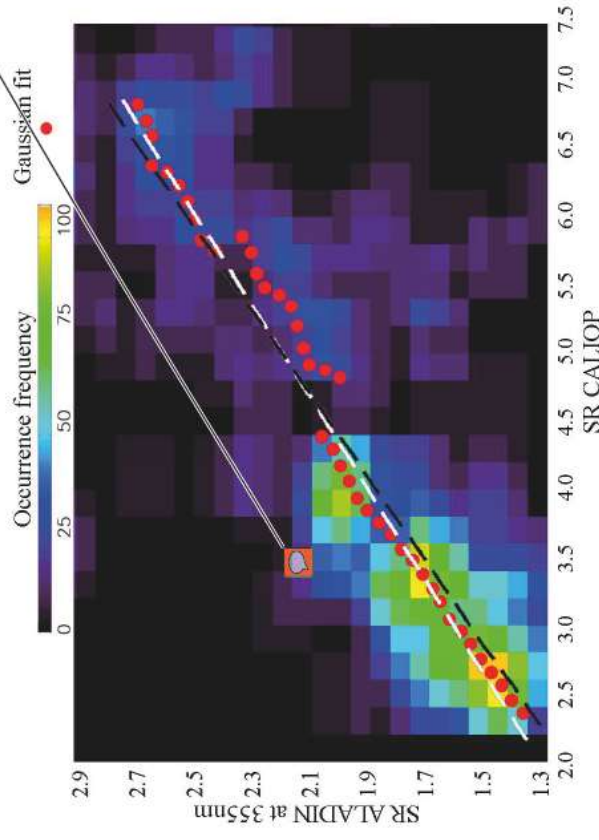


Figure A1: Correlation between individual pairs of CALIOP and ALADIN scattering ratio profiles, for all altitudes. The colors of the bins represent the occurrence frequencies for 0.2×0.07 SR bins, as a function of both CALIOP's $SR_{0.2}$ and ALADIN's $SR_{0.2}$. For each point along the diagonal, a Gaussian was fitted to the data points lying along a perpendicular transect and the central point of the Gaussian is plotted as a red filled circle. The white dashed line represents a linear fit to these points. For comparison, black dashed line shows the fit given by Eq. 1.

AC: this Figure does not exist in the new version. As for the question, we wanted to check the conversion itself, regardless of the SR threshold used later.